Sensors & Transducers, Vol. 239, Issue 12, December 2019, pp. 47-55

www.sensorsportal.com

Sensors & Transducers

Published by IFSA Publishing, S. L., 2019
http://www.sensorsportal.com

Analysis of Material Dependent Thermoelastic Damping Limited Critical Thickness in Micro/Nanobeams

[1, 2 *] Resmi R., [1] M. R. Baiju and [1] V. Suresh Babu
[1] Kerala University, India
[2] LBS Institute of Technology for Women, Poojappura, India
[*] Tel.: 009446136613
E-mail: resmilbs@gmail.com

Received: 19 September 2019 /Accepted: 30 November 2019 /Published: 9 December 2019

Abstract: The thermoelastic energy dissipation of micro/nano beam resonators is a critical energy loss mechanism which limits the maximum attainable quality factor. Critical thickness of a resonator is defined as the thickness at which the peaking of energy takes place. The critical dimensions of the resonators are properly selected to alleviate the energy losses i.e. by properly selecting the thickness of the resonators the peaking of energy dissipation can be alleviated. Classical continuum theories cannot explain the size effect related to mechanical behavior at micron or submicron sizes. In this study, isotropic rectangular micro-plates are used to analyze the size-dependent thermoelastic damping and its impact on the critical thickness. Micro- and nanoplates using five different structural materials are analyzed to optimize *hc*, which depends on thermal diffusion length l_T of the material. In our study, an expression for the theroelastic damping limited quality factor is obtained in terms of the material performance indices and simulated numerically. In this work, h_{cmax} is obtained for resonators with Si material, which has the highest l_T. The impact of length-scale parameters (l), vibration modes, boundary conditions, and operating temperatures on *hc* are also investigated. It is concluded that *hc* is maximized by selecting Si as the structural material with higher internal length-scale parameters (l). These results can help designers to engineer high-performance, low-loss resonators.

Keywords: Modified coupled stress theory, Micro/nanobeam resonators, Material length scale parameter, Quality factor, Thermoelastic damping.

1. Introduction

Micro- and nanoelectromechanical systems (MEMS and NEMS) based thin beams are one of the major structures emerged as the essential components for sensing [1] and communication applications [2]. Most of these applications exploited the mechanical and thermal properties of thin film materials for focused applications as in micro switches [3] , micro mirrors [4],microphones [5], micro-pumps [6], shock sensors [7], biosensors [8], resonators [9], atomic force microscopes [10], actuators [11, 12] etc. Micro/nano beams are universally used due to their advantages of high reliability, improved sensitivity, reduced size, mass and cost, high surface-to-volume ratio etc. [13].

One of the salient features of resonators used mainly as sensors and filters is its Quality Factor (QF) which gives a representation of expended energy due to its various energy dissipation methods which can be classified as extrinsic and intrinsic[14]. As the dissipated energy increases QF declines which deteriorates the sensitivity, resolution and reliability of micro/nano devices [15]. Extrinsic losses can be easily managed whereas to mitigate intrinsic losses proper design of the device structure with geometry

and material optimization and appropriate boundary condition selection etc. should be done. Thermoelastic damping is a crucial intrinsic energy dissipation mechanism at micro and nano-scales which limits the maximum achievable QF in the resonator denoted by Q_{TED} [16].

Presence of TED in different structures is identified in various research works. Thermoelastic damping in rotating flexible micro-disk [17], rings [18], thick beams [19], rectangular and circular microplate resonator [20], bi-layered micro-plates [21] and laminated composite micromechanical beam resonators [22] are reported. In order to manage with the increasing demands toward developing microstructures of high quality factors, several optimizations are made based on geometry, materials and operating conditions. The Q_{TED} can be improved by properly selecting the dimensions, materials, boundary conditions and operating temperature of the device. This work aims to mitigate thermoelastic damping by optimizing the material, vibrating mode, boundary condition and internal length scale parameter by applying Modified coupled Stress Theory.

Zener identified the existence of TED as a prominent energy loss mechanism in homogeneous, isotropic, Euler–Bernoulli micro-beams in 1937 [23-25]. Roszhart T. Vstudied the effect of thermoelastic internal friction on the Q of micro-machined silicon resonators [26]. Lifshitz and Roukes derived an exact closed-form expression for TED of slender beams and studied the effect of different geometrical parameters [27]. Prabhakar and Vengallatore analyzed TED with two-dimensional heat transfer and presented an analytical relation for TED in the form of an infinite series for micro-resonators [28]. Sharma and Kaur studied transverse vibrations in thin micro beams based on Euler-Bernoulli theory under clamped-clamped boundary conditions [29]. Srikar and Sairam [30] investigated the frequency dependence of TED in asymmetric, bilayered, micromechanical Euler-Bernoulli beam resonators without considering the effect of additional layers thickness for materials with no electro-mechanical coupling coefficient. Rezazadeh reported that the stiffness of the resonator is altered by applying DC voltages to the piezoelectric layers; and the effect of electromechanical coupling of piezoelectric materials on TED is studied [31]. Srikar and Senturia suggested that single-crystal Silicon, rather than fine-grained Polysilicon, is the material of choice for making flexural beam resonators in the gigahertz frequency range [16]. Evoy [32] and Duwel [33] showed experimentally that TED is a dominant source of damping in MEMS and NEMS devices. Parayil presented analytical and numerical solutions for TED of Timoshenko microbeams [19]. Nourmohammadi [34] investigated nonlinear TED by estimating the expended energy per cycle of vibration in microbeams by solving the nonlinear coupled equations utilizing the finite difference method.

The behaviour of materials change as the size of the structures is scaled down and these size effects has been proved experimentally [35]. Size effect in gold microstructures was experimentally shown under tensile compressive and bending [36] tests. The size effect in engineering materials was first studied in the works of Cauchy [37] and Voigt [38] and included the analysis of the physical phenomena. Voigt's works included an extensive approach containing kinematics, balance laws and constitutive relations. Analysis of TED in micro/nanobeams based on Classical continuum theories are insufficient to predict the size-dependent mechanical behavior [35-39] due to the lack of material length scale parameter and hence higher order continuum theories can be used to estimate the size dependencies at micron/submicron levels.

Yang et al [40] developed modified couple stress theory in which only a single material length scale parameter is involved besides two classical material constants to investigate the mechanical behaviour of microstructures such as microbeams, microplates, and microshells [41]. The strain energy has been shown to be a quadratic function of the symmetric strains and the symmetric curvatures. The main advantage of MCST is it is much easier to deal with a single material length scale parameter so that computational efficiency is high. Fathalilou [42] used the modified couple stress theory to study the pull-in instability of a gold microbeam switch. Rahaeifar [43] investigated the size effect on the deflection and static pull-in voltage using the MCST. Shaat and Mohamed [44] considered surface effects which are incorporated into the modified couple stress model to in estimating the electrostatic and the pull-in instability behaviours of microactuated beams. Shaat [44] conducted bending analysis for Size-dependent Kirchhoff nano-plates incorporating surface effects based on a MCST. By applying MCST, Rezazadeh derived a size-dependent relation for TED in microbeams and studied the small-scale effects on the critical thickness. Taati [45] developed some models for the transient analysis of coupled thermoelasticity of microbeams.

This manuscript is organized as follows: In Section 2, introduction to higher-order theories based on variational principles is given. Section 3 is devoted to derive Q_{TED} from equations of motion and coupled thermoelasticity for micro-beams. In Section 4, numerical analysis is done to demonstrate the effect of MCST and coupled thermoelasticity on h_c of beams with different structural materials. The impact of size effect, boundary conditions, vibration modes and plane stress/plane strain conditions with different structural materials are analyzed in detail. Section 5 includes concluding remarks.

2. Formulation of Basic Equations of a Beam Resonator Applying Non-classical Elasticity Theory

2.1. Stress and Strain Fields in a Vibrating Microbeam

The displacements in the x and z directions of a beam are analyzed according to the Euler-Bernoulli model based assumptions. Longitudinal displacement $u_x(x,z,t)$in terms of transversal displacement is $u_z(x,t)$ is expressed as

$$u_x = -zu_{z,x} \tag{1}$$

During vibrations of the beam, coupling of temperature and elastic fields occur and as a result deformations due to thermal and mechanical components arise.

Mechanical strain:

$$\varepsilon_{ij}(M) = \frac{n}{E}\sigma_{ij} - \frac{v}{E}\sigma_{kk}\delta_{ij} = \frac{n}{E}\sigma_{ij} + \frac{m-n}{2E}\sigma_{kk}\delta_{ij}, \tag{2}$$

in which σ_{ij}, δ_{ij} and E are the conventional symbols used for stress tensor, the Kronecker delta and Young's modulus, respectively. In addition to the conventional parameters, two new material dependent parameters m and $n$are derived from Poisson's ratio.

Thermal strain:

$$\varepsilon_{ij}(T) = \alpha\vartheta\delta_{ij}, \tag{3}$$

where α is the thermal expansion coefficient and $\vartheta = T - T_0$ is the temperature change with respect to a reference temperature T_0 and assuming shear strains created by temperature change are negligible. Considering Eqns. (1), (2) and (3), the total strain field,

$$\begin{aligned}\varepsilon_{ij} &= \frac{n}{E}\sigma_{ij} + \left(\alpha\vartheta - \frac{v}{E}\sigma_{kk}\right)\delta_{ij} \\ &= \frac{n}{E}\sigma_{ij} + \left(\alpha\vartheta + \frac{m-n}{2E}\sigma_{kk}\right)\delta_{ij}\end{aligned} \tag{4}$$

3. Thermoelastic Damping Limited Quality Factor of a Beam Resonator with Material Length Scale Parameter

For coupled thermoelastic damping equations, the following solutions for the beam deflection and temperature distribution are assumed:

$$u_z(x,t) = W(x)e^{st}$$

and

$$\vartheta(x,z,t) = \vartheta_0(x,z)e^{st}, \tag{5}$$

where $s = \overline{\omega} + i\omega$.

Under the plane stress condition:

$$\vartheta_{0,zz} = \frac{s}{\chi}\left[\left(1 + 2\acute{r}\frac{n}{p}\right)\vartheta_0 - \frac{\acute{r}}{\alpha}zW_{,xx}\right] \tag{6}$$

The solution is

$$\vartheta_0(x,z) = \frac{\acute{r}}{\alpha\left(1+2\acute{r}\frac{n}{p}\right)}zW_{,xx} + C_1e^{gz} + C_2e^{-gz}, \tag{7}$$

where

$$g = \left(\left(1 + 2\acute{r}\frac{n}{p}\right)s/\chi\right)^{1/2} \tag{8}$$

Assuming adiabatic condition

$$\vartheta_0(x,z) = \frac{\acute{r}}{\alpha\left(1 + 2\acute{r}\frac{n}{p}\right)}W_{,xx}\left[z - \frac{\sinh(gz)}{g\cosh\left(g\frac{h}{2}\right)}\right]$$

Considering thermoelastic damping, isothermal value of Young's modulus is replaced by

$$\widehat{EI}(s,l) = (EI)_{eq}\left\{1 + \frac{\acute{r}}{\mathfrak{B}}\left(1 + 2\acute{r}\frac{n}{p}\right)[1 + f(s)]\right\} \tag{9}$$

The isothermal value of s is

$$s_{iso} = \pm i\omega_{iso}, \tag{10}$$

where

$$\omega_{iso} = \left(\frac{a_n}{L}\right)^2\sqrt{\frac{(EI)_{eq}}{\rho A}}, \tag{11}$$

$$a_n = \begin{cases} 4.730, 7.853, 10.996 & for clamped-clamped \\ 3.1417, 6.2849, 9.4234 & for simply supported \\ 3.52, 4.694, 7.855 & for cantilever \end{cases} \tag{12}$$

and

$$s = \pm i\left(\frac{a_n}{L}\right)^2\sqrt{\frac{\widehat{EI}(s,l)}{\rho A}} \tag{13}$$

$$= s_{iso}\sqrt{1 + \frac{\acute{r}}{\mathfrak{B}\left(1 + 2\acute{r}\frac{n}{p}\right)}[1 + f(s)]}$$

$$= s_{iso}\left\{1+\frac{1}{2}\frac{ŕ}{\mathfrak{B}\left(1+2ŕ\frac{n}{p}\right)}[1+f(s_{iso})]\right\} \quad (14)$$

$$= s_{iso}\Omega$$

$$\mathfrak{R}(\Omega) = 1+\frac{1}{2}\frac{ŕ}{\mathfrak{B}\left(1+2ŕ\frac{n}{p}\right)}\left(1-\frac{6}{\xi'^3}\frac{\sinh(\xi')-\sin(\xi')}{\cosh(\xi')+\cos(\xi')}\right) \quad (15)$$

$$\mathfrak{I}(\Omega) = \frac{1}{2}\frac{ŕ}{\mathfrak{B}\left(1+2ŕ\frac{n}{p}\right)}\left(\frac{6}{\xi'^2}-\frac{6}{\xi'^3}\frac{\sinh(\xi')+\sin(\xi')}{\cosh(\xi')+\cos(\xi')}\right), \quad (16)$$

where

$$\xi' = h\sqrt{\frac{\left(1+2ŕ\frac{n}{p}\right)\omega_{iso}}{2\chi}} \quad (17)$$

The inverse of the quality factor

$$Q^{-1} = 2\left|\frac{\mathfrak{R}(s)}{\mathfrak{I}(s)}\right| = 2\left|\frac{\mathfrak{R}(\Omega)}{\mathfrak{I}(\Omega)}\right| \quad (18)$$

$$Q^{-1}_{MCST} = \frac{Q^{-1}_{CT}}{\mathfrak{B}} \quad (19)$$

$$Q^{-1}_{CT} = \frac{ŕ}{\left(1+2ŕ\frac{n}{p}\right)}\left(\frac{6}{\xi'^2}-\frac{6}{\xi'^3}\frac{\sinh(\xi')+\sin(\xi')}{\cosh(\xi')+\cos(\xi')}\right) \quad (20)$$

$$Q^{-1}_{LR} = ŕ\left(\frac{6}{\xi^2}-\frac{6}{\xi^3}\frac{\sinh(\xi)+\sin(\xi)}{\cosh(\xi)+\cos(\xi)}\right) \quad (21)$$

in which $\xi = h\sqrt{\omega_{iso}/2\chi}$

$$(Q^{-1}_{MCST})^* = \frac{ŕ}{\mathfrak{B}^*\left(1+\frac{ŕn}{mp}\right)}\left(\frac{6}{\xi^{*2}}-\frac{6}{\xi^{*3}}\frac{\sinh(\xi^*)+\sin(\xi^*)}{\cosh(\xi^*)+\cos(\xi^*)}\right), \quad (22)$$

where

$$\mathfrak{B}^* = \frac{(EI)^*_{eq}}{(EI)^*} \quad (23)$$

$$(EI)^*_{eq} = \left(\frac{EI}{mn}+\mu Al^2\right) \quad (24)$$

$$\xi^* = h\frac{\left(1+\frac{ŕn}{mp}\right)\omega^*_{iso}}{2\chi} \quad (25)$$

$$\omega^*_{iso} = \left(\frac{a_n}{L}\right)^2\sqrt{\frac{(EI)^*_{eq}}{\rho A}} \quad (26)$$

4. Results and Discussions

For validating the analytical study, critical thickness, h_c of micro/nanobeam resonators using five different structural materials are numerically simulated using MATLAB 2015a. The experimentally reported mechanical and thermodynamic properties of all the materials are given in Table 1. The different boundary conditions selected for analysis are simply supported, clamped-clamped and cantilever beams vibrating in the first three modes. In Section 4.1 the various factors affecting hc are analyzed and Section 4.2 deals with the impacts of different conditions such as material performance index, material length scale parameter, boundary conditions and mode switching on h_c.

Table 1. Mechanical and thermal properties of different materials.

Properties	PolySi	Diamond	Si	GaAs	SiC
E[GPa]	150	800	130	85.9	415
v	0.226	0.069	0.28	0.31	0.192
ρ	2328	3515	2230	5316	3200
k	40	100	90	52	70
C_p	713	510	699	550	937.5
$\alpha[10^{-6}]$	2.3	1.2	2.59	5.73	3.0
$\chi[cm^2/s]$	0.241	0.558	0.577	0.178	0.233
C_v	1659864	1792650	1558770	2923800	3000000

In this paper, the important performance measuring criteria selected for analysis is critical thickness, hc of the device which is found to be affected by thermal diffusion length, ℓ_T of the material as shown in Table 2.

As mode increases the critical thickness of the beam decreases in the order Mode-I> Mode-II > Mode-III. When the length scale parameter increases the critical thickness of the beam is almost constant. The different boundary conditions taken for analysis are simply supported ,clamped-clamped and cantilever cases and the order in which h_c changes with boundary conditions is $h_{c\ SS}$> $h_{c\ CL}$> $h_{c\ CC}$. The critical thickness for plane stress and plane strain condition is almost constant but in some cases, there is a slight variation in between them such that h_c plane stress > h_c plane strain.

Table 3 shows the critical thickness of different materials vibrating in first mode.

Table 2. Material Dependent Performance Indices for Micro/Nano beams.

Parameters	PolySi	Diamond	Si	GaAs	SiC
$\acute{r}(10^{-4})$	1.43	2.26	1.68	2.9	3.74
$\ell_T(nm)$	3	3.69	7.56	4.42	2.04
m^{*}	0.774	0.931	0.72	0.69	0.808
n^{**}	1.226	1.069	1.28	1.31	1.192
p^{***}	0.548	0.862	0.44	0.38	0.616

*(1-v), ** (1+v), *** (1- 2v)

Table 3. Critical thickness (μm) of different materials in Mode-I.

STRESS/ STRAIN	l(μm)	B.C	PolySi	Diamond	Si	GaAs	SiC
PLANE STRESS	0	CC	3.601	3.801	4.901	4.101	3.201
		SS	4.701	5.001	6.401	5.401	4.101
		CL	4.401	4.701	5.901	5.001	3.801
	0.2	CC	3.601	3.801	4.901	4.101	3.201
		SS	4.701	5.001	6.401	5.401	4.101
		CL	4.401	4.701	5.901	5.001	3.801
	0.5	CC	3.601	3.901	4.901	4.101	3.201
		SS	4.701	5.101	6.401	5.401	4.201
		CL	4.401	4.701	5.901	5.001	3.901
	1	CC	3.601	3.901	4.901	4.101	3.201
		SS	4.801	5.101	6.401	5.401	4.201
		CL	4.401	4.701	6.001	5.001	3.901
PLANE STRAIN	0	CC	3.601	3.801	4.801	4.001	3.101
		SS	4.701	5.001	6.301	5.301	4.101
		CL	4.301	4.701	5.901	4.901	3.801
	0.2	CC	3.601	3.801	4.801	4.001	3.101
		SS	4.701	5.001	6.401	5.401	4.101
		CL	4.301	4.701	5.901	4.901	3.801
	0.5	CC	3.601	3.901	4.801	4.001	3.201
		SS	4.701	5.101	6.301	5.301	4.101
		CL	4.301	4.701	5.901	4.901	3.801
	1	CC	3.601	3.901	4.801	4.101	3.201
		SS	4.701	5.101	6.301	5.301	4.201
		CL	4.401	4.701	5.901	4.901	3.901

4.1. Effect of Material Performance Index

The critical thickness, h_c depends on thermal diffusion length, ℓ_T of the material as shown in Table 2. The order in which h_c diminishes is Si > GaAs > Diamond > PolySi > SiC which is directly proportional to the thermal diffusion length of the material. As the material length scale parameter increases critical thickness increases slightly. Maximum value of critical thickness is attained for Si (6.401 μm) and minimum is obtained for SiC (1.801 μm).

Fig. 1 and Fig. 2 represent the normalized energy dissipation of different materials when length scale parameter becomes 1 μm. Fig. 1 and 2 represents the stress and strain conditions of the beam respectively under Clamped-Clamped boundary condition.

From Fig. 1, the maximum critical thickness (4.901 μm) is obtained for Si under plane stress condition. The maximum critical thickness under plane strain condition is obtained for Si (4.801 μm) as shown in Fig.2.

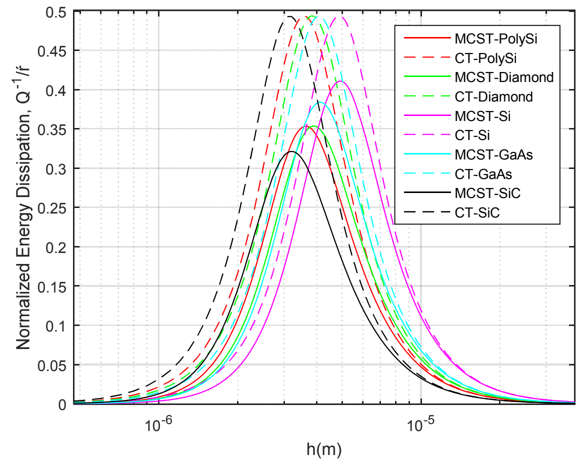

Fig. 1. Normalized energy dissipation Vs thickness of a beam under plane stress condition.

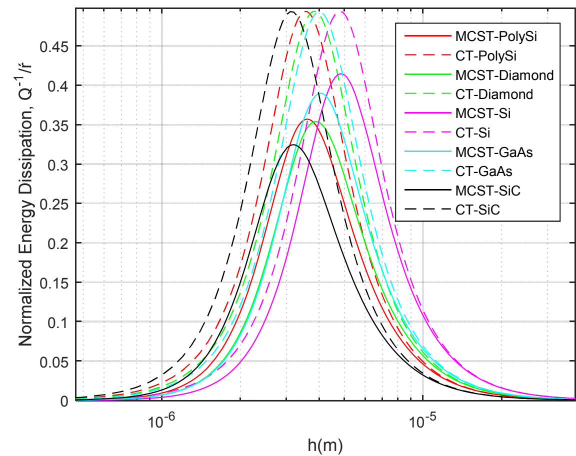

Fig. 2. Normalized energy dissipation Vs thickness of a beam under plane strain condition.

4.2. Effect of Material Length Scale Parameters

Fig. 3 and Fig. 4 show the comparison of critical thickness for different length scale parameters when Si is used as the structural material. Fig. 3 and Fig. 4 corresponds to the plane stress condition and the plane strain condition respectively. Clamped-clamped boundary condition in first vibration mode is plotted

in Fig. 3 and Fig. 4. From Fig. 3 and Fig. 4, the maximum critical thickness 3.20 µm is obtained with *l*=0 µm.

The maximum percentage difference due to size effect (5.55 %) is obtained between *l*=0 and *l*=1; the order of percentage change is SiC >polySi> diamond >GaAs>Si, and depends mainly on the material parameter υ. The maximum percentage difference was obtained for SiC microplates, and the minimum was found for Si microplates.

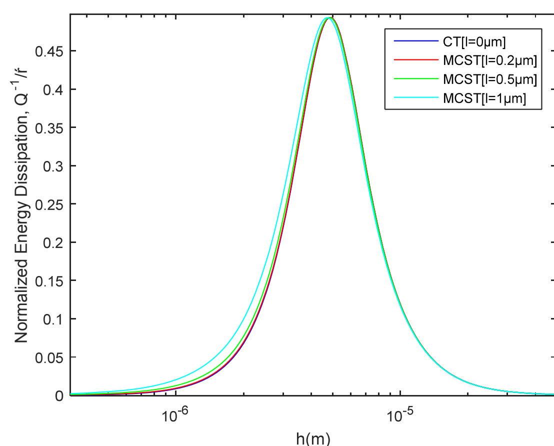

Fig. 3. Comparison of critical thickness based on Si of different length scale parameters under plane stress condition.

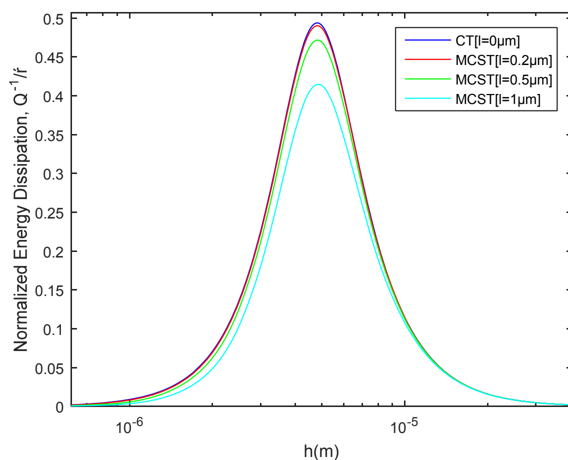

Fig. 4. Comparison of critical thickness based on Si of different length scale parameters under plane strain condition.

4.3. Effect of Boundary Conditions

The boundary conditions taken for analysis are the simply supported, clamped-clamped and cantilever cases using different structural materials. In the case of different boundary conditions, maximum critical thickness is obtained for simply supported case and the minimum is for clamped–clamped condition. The boundary condition order in which h_c varies is h_c(SS) >h_c(CL) >h_c(CC).

Fig. 5 and Fig. 6 represent the comparison of different boundary conditions based on polySi material in first vibration mode with different length scale parameters. The beam under plane stress and plane strain conditions are shown in Fig. 5 and 6 respectively. The maximum critical thickness (4.701µm) is obtained for simply supported boundary condition with *l*=0 µm.

The maximum percentage change (45.43 %) of h_c in accordance with boundary condition is obtained in between clamped-clamped and cantilever conditions vibrating in second mode with *l*=0µm. The order of materials is SiC > diamond > GaAs > Si>polySi. The minimum percentage difference (5.99 %) of h_c in accordance with boundary condition obtained is in between simply supported and cantilever vibrating in first mode with *l*=1 µm.

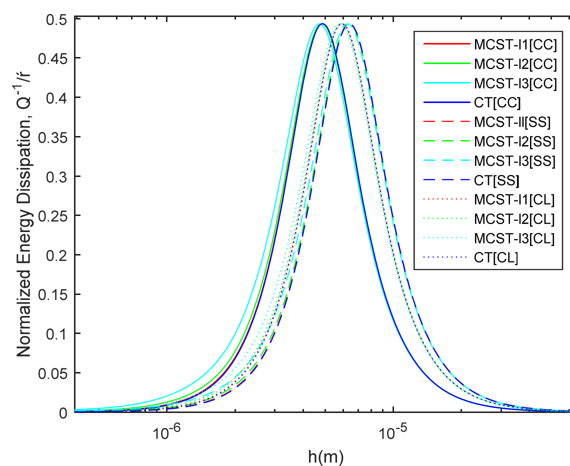

Fig. 5. Comparison of critical thickness for Si of different boundary conditions under plane stress condition.

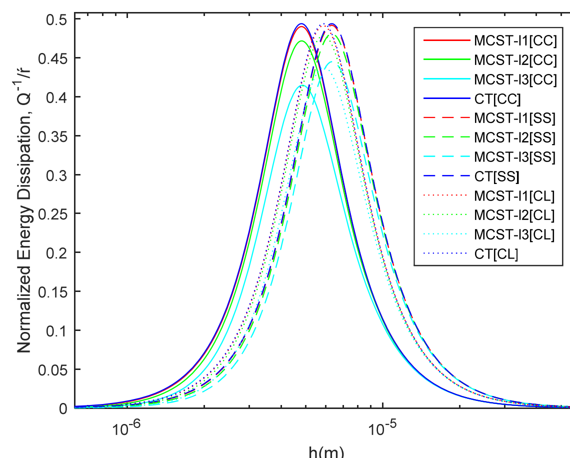

Fig. 6. Comparison of critical thickness for Si of different boundary conditions under plane strain condition.

4.4. Effect of Mode Switching

As the mode number increases h_c decreases.

Table 4 shows the critical thickness of different materials under second vibration mode condition.

Table 5 shows the critical thickness of different materials under third vibration mode condition.

Table 4. Critical thickness (µm) of different materials in Mode-II.

STRESS/ STRAIN	*l*(µm)	B.C	PolySi	Diamond	Si	GaAs	SiC
PLANE STRESS	0	CC	2.601	2.701	3.501	2.901	2.201
		SS	3.001	3.201	4.001	3.401	2.601
		CL	3.601	3.901	4.901	4.101	3.201
	0.2	CC	2.601	2.701	3.501	2.901	2.301
		SS	3.001	3.201	4.001	3.401	2.601
		CL	3.601	3.901	4.901	4.101	3.201
	0.5	CC	2.601	2.801	3.501	2.901	2.301
		SS	3.001	3.201	4.001	3.401	2.601
		CL	3.601	3.901	4.901	4.101	3.201
	1	CC	2.601	2.801	3.501	3.001	2.301
		SS	3.001	3.201	4.101	3.401	2.701
		CL	3.601	3.901	4.901	4.101	3.201
PLANE STRAIN	0	CC	2.501	2.701	3.401	2.901	2.201
		SS	2.901	3.201	4.001	3.301	2.601
		CL	3.601	3.901	4.801	4.001	3.101
	0.2	CC	2.501	2.701	3.401	2.901	2.201
		SS	2.901	3.201	4.001	3.301	2.601
		CL	3.601	3.901	4.801	4.001	3.201
	0.5	CC	2.601	2.801	3.401	2.901	2.301
		SS	3.001	3.201	4.001	3.301	2.601
		CL	3.601	3.901	4.801	4.001	3.201
	1	CC	2.601	2.801	3.501	2.901	2.301
		SS	3.001	3.201	4.001	3.401	2.701
		CL	3.601	3.901	4.901	4.101	3.201

By considering the percentage change of critical thickness between modes, the maximum change (52.36 %) is obtained in between first and third vibrating modes under simply supported condition with *l*=1 µm. The order of materials for maximum change is SiC > GaAs > Si > polySi > diamond. The minimum percentage difference (15.78 %) is obtained in between first and second vibrating modes of a cantilever beam with *l*=0 µm. The maximum and minimum percentage change of critical thickness between modes is same for both plane stress and plane strain conditions.

Fig. 7 and Fig. 8 represent the comparison of critical thickness for different modes based on SiC material. Fig. 6 and Fig. 7 represent the plane stress and plane strain conditions of beam respectively. The clamped-clamped boundary condition with different length scale parameters is given in Fig. 6 and Fig. 7. From Fig. 6 and Fig. 7, the maximum critical thickness 3.201 µm is obtained in first vibrating mode with *l*=0 µm.

Table 5. Critical thickness (µm) of different materials in Mode-III.

STRESS/ STRAIN	*l*(µm)	B.C	PolySi	Diamond	Si	GaAs	SiC
PLANE STRESS	0	CC	2.001	2.201	2.801	2.301	1.801
		SS	2.301	2.401	3.101	2.601	2.001
		CL	2.601	2.701	3.501	2.901	2.201
	0.2	CC	2.001	2.201	2.801	2.301	1.801
		SS	2.301	2.401	3.101	2.601	2.001
		CL	2.601	2.701	3.501	2.901	2.301
	0.5	CC	2.101	2.201	2.801	2.301	1.801
		SS	2.301	2.501	3.101	2.601	2.001
		CL	2.601	2.801	3.501	2.901	2.301
	1	CC	2.101	2.301	2.801	2.401	1.901
		SS	2.301	2.501	3.101	2.601	2.101
		CL	2.601	2.801	3.501	3.001	2.301
PLANE STRAIN	0	CC	2.001	2.201	2.701	2.301	1.801
		SS	2.201	2.401	3.001	2.501	2.001
		CL	2.501	2.701	3.401	2.901	2.201
	0.2	CC	2.001	2.201	2.701	2.301	1.801
		SS	2.201	2.401	3.001	2.501	2.001
		CL	2.501	2.701	3.401	2.901	2.201
	0.5	CC	2.001	2.201	2.801	2.301	1.801
		SS	2.301	2.401	3.101	2.601	2.001
		CL	2.601	2.801	3.401	2.901	2.301
	1	CC	2.101	2.301	2.801	2.301	1.801
		SS	2.301	2.501	3.101	2.601	2.001
		CL	2.601	2.801	3.501	2.901	2.301

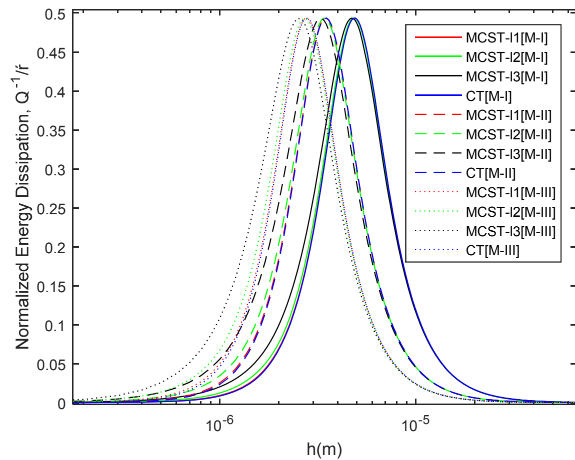

Fig. 7. Comparison of critical thickness for SiC of different modes under plane stress condition.

4.5. Effect of Plane Stress and Plane Strain Conditions

The critical thickness for beam resonators with plane stress condition is slightly greater than that for beam resonators with plane strain beam in certain cases.

By considering the percentage change between stress and strain, the maximum change is obtained for SiC (5.26 %) of clamped-clamped boundary condition with l=1μm. There is no significance for the minimum percentage change between the plane stress and plane strain condition.

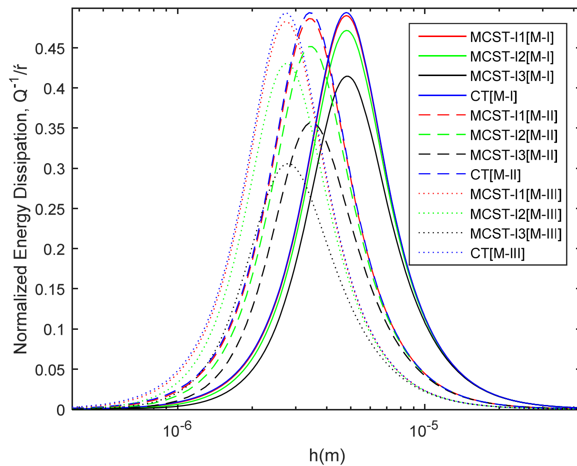

Fig. 8. Comparison of critical thickness for SiC of different modes under plane strain condition.

Fig. 9 shows the comparison of critical thickness under stress and strain conditions of different materials respectively. The maximum h_c (4.901 μm) is obtained for a clamped-clamped Si beam with l=1 μm vibrating in first mode.

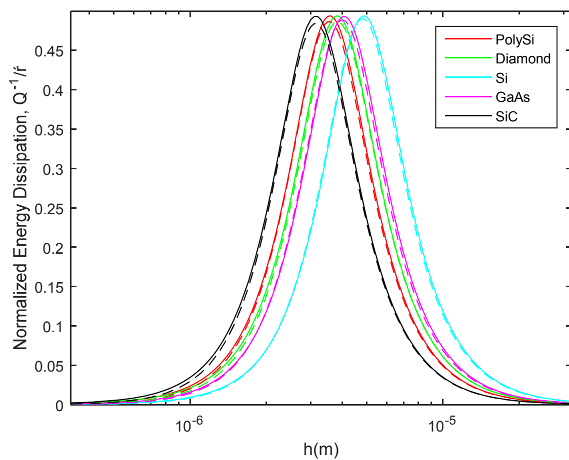

Fig. 9. Comparison of critical thickness of different materials under plane stress and plane strain condition [− plane stress, - - plane strain].

7. Conclusions

In this study, micro/nanobeams based on the Euler-Bernoulli beam model applying MCST are used to analyze size-dependent TED and its impact on critical thickness. Five different structural materials are used for optimizing *hc*, which depend on the diffusion length l_T. According to this work, the maximum critical thickness, h_{cmax} is obtained for Si, which has the highest l_T. The critical thickness for plane stress and plane strain condition is almost constant .When the mode number is increased, *hc* decreases in the order Mode-I> Mode-II > Mode-III. As the material length scale parameter (l) increases, *hc* is almost constant. The order in which h_c changes with boundary conditions is $h_{c\ SS}$> $h_{c\ CL}$> $h_{c\ CC}$. The prior knowledge of *hc* can help engineers to design high performance, low loss resonators.

References

[1]. Chen J. Y., Hsu Y. C., Lee S. S., Mukherjee T., Fedder G. K., Modeling and simulation of a condenser microphone, *Sensors and Actuators A*, 145–146, 2008, pp. 224-230.

[2]. M. Gologanu, C. G. Bostan, V. Avramescu, O. Buiu, Damping Effects in MEMS Resonators, in *Proceedings of the International IEEE Semiconductor Conference (CAS 2012)*, 2012, pp. 67-74.

[3]. Zhang, Y. H., Ding, G., Shun, X., Gu, D., Cai, B., Lai, Z., Preparing of a high speed bistable electromagnetic RF MEMS switch, *Sens. Actuat. A,* 134, 2, 2007, pp. 532–537.

[4]. Rezazadeh G., Khatami F., Tahmasebi A., Investigation of the torsion and bending effects on static stability of electrostatic torsional micromirrors, *Microsystem Technologies,* 13, 2007, pp. 715-722.

[5]. Liu J., Martinn D. T., Kardirvel K., Nishida T., Cattafesta L., Sheplak M., Mann B., Nonlinear model and system identification of a capacitive dual-back plate MEMS microphone, *Journal of Sound and Vibration,* 309, 2008, pp. 276-292.

[6]. Saif M. T. A., Alaca B. E., Sehitoglu H., Analytical modeling of electrostatic membrane actuator micropumps, *Journal of Microelectromechanical Systems*, 8, 1999, pp. 335–345.

[7]. M. I. Younis, F. Alsaleem, D. Jordy, The response of clamped–clamped microbeams under mechanical shock, *International Journal Nonlinear Mech.,* 42, 2007, pp. 643–657.

[8]. Eom, K., Kwon, T. Y., Yoon, D. S., Lee, H. L., Kim, T. S., Dynamical response of nanomechanical-resonators to biomolecular interactions, *Phys. Rev. B,* 76, 11, 2007, 113408.

[9]. Lee, I., Lee, J., Measurement uncertainties in resonant characteristics of MEMS resonators, *J. Mech. Sci. Technol.,* 27, 2, 2013, pp. 491–500.

[10]. W. L. Wang, S. J. Hu, Modal response and frequency shift of the cantilever in a noncontact atomic force microscope, *Applied Physics Letters*, 87, 18, 2005, 183506.

[11]. Tilmans H. A., Legtenberg R., Electrostatically driven vacuum-encapsulated polysilicon resonators, Part II, Theory and performance, *Sensors and Actuators A*, 45, 1994, pp. 67-84.

[12]. R. E. Mihailovich and N. C. MasDonald, Dissipation measurements of vacuum-operated single-crystal silicon micro resonators, *Sens. Actuat. A. Phys.*, Vol. 50, No. 3, 1995, pp. 199–207.

[13]. K. Tunvir, C. Q. Ru, and A. Mioduchowski, Effect of cross-sectional shape on thermoelastic dissipation of

micro/nano elastic beams, *Inter. J. Mech. Sci.,* Vol. 62, 2012, pp. 77–88.

[14]. Yang, J., Ono, T., Esashi, M., Energy dissipation in submicrometer thick single-crystal silicon cantilevers, *J. Microelectromech. Syst.,* 11, 6, 2002, pp. 775–783.

[15]. Kakhki, E. K., Hosseini, S. M., Tahani, M., An analytical solution for thermoelastic damping in a micro-beam based on generalized theory of thermoelasticity and modified couple stress theory, *Appl. Math. Model.,* 40, 4, 2016, pp. 3164–3174.

[16]. V. T. Srikar and S. D. Senturia, Thermoelastic damping in fine grained polysilicon flexural beam resonators, *J. Microelectromech. Syst*., Vol. 11, No. 5, 2002, pp. 499–504.

[17]. Pei, Y. C., Thermoelastic damping in rotating flexible micro-disk, *Int. J. Mech. Sci.,* 61, 1, 2012, pp. 52–64.

[18]. Hossain, S. T., McWilliam, S., Popov, A. A., An investigation on thermoelastic damping of high-Q ring resonators, *Int. J. Mech. Sci.,* 106, 2016, pp. 209–219.

[19]. Parayil, D. V., Kulkarni, S. S., Pawaskar, D. N., Analytical and numerical solutions for thick beams with thermoelastic damping, *Int. J. Mech. Sci.*, 94, 2015, pp. 10–19.

[20]. Fang, Y., Li, P., Zhou, H., Zuo, W., Thermoelastic damping in rectangular microplate resonators with three-dimensional heat conduction, *Int. J. Mech. Sci.,* 133, 2017, pp. 578–589.

[21]. Liu, S., Sun, Y., Ma, J., Yang, J., Theoretical analysis of thermoelastic damping in bilayered circular plate resonators with two-dimensional heat conduction, *Int. J. Mech. Sci.* 135, 2018, pp. 114–123.

[22]. Srikar Vengallatore, Analysis of thermoelastic damping in laminated composite micromechanical beam resonators, *J. Micromech. Microengg.*, 15, 12, 2005, pp. 2398-2404.

[23]. Zener, C., Internal friction in solids. I. Theory of internal friction in reeds, *Phys. Rev.* 52, 1937, 230.

[24]. Zener, C., Internal friction in solids II. General theory of thermoelastic internal friction, *Phys. Rev.,* 53, 1, 1938, pp. 90–99.

[25]. Zener, C., Elasticity and An elasticity of Metals, *University of Chicago Press*, Chicago, Illinois, 1948.

[26]. Roszhart, T. V., The effect of thermoelastic internal friction on the Q of micromachined silicon resonators, in *Proceedings of the IEEE 4th Technical Digest on Solid-State Sensor and Actuator Workshop*, 1990, pp. 13–16.

[27]. Lifshitz, R., Roukes, M. L., Thermoelastic damping in micro-and nanomechanical systems, *Phys. Rev. B*, 61, 8, 2000, pp. 5600-5609.

[28]. Prabhakar, S., Vengallatore, S., Theory of thermoelastic damping in micromechanical resonators with two-dimensional heat conduction, *J. Microelectromech. Syst.,* 17, 2, 2008, 494–502.

[29]. Sharma, J. N. and Kaur, R., Transverse vibrations in thermoelastic-diffusive thin microbeamresonators, *J. Thermal Stresses,* Vol. 37, 2014, pp. 1265-1285.

[30]. Sairam, P. and Srikar, V., Thermoelastic damping in bilayered micromechanical beam resonator, *J. Micromechanic Microengineering,* 2007, 17, 3, pp. 532-538.

[31]. Rezazadeh, G., Tahmasebi, A., Zubstov, M., Application of piezoelectric layers in electrostatic MEM actuators: controlling of pull-in voltage, *Microsyst. Technol.,* 12, 2006, pp. 1163–1170.

[32]. Evoy, S., Oikhovets, A., Sekaric, L., Parpia, J. M., Craighead, H. G., Carr, D. W., Temperature-dependent internal friction in silicon nano-electromechanical systems, *Appl. Phys. Lett.*, 77, 2000, pp. 2397–2399.

[33]. A. Duwel, R. N. Candler, T. W. Kenny, and M. Varghese, Engineering MEMS resonators with low thermoelastic damping, *J. Microelectromech. Syst.,* Vol. 15, No. 6, 2006, pp. 1437–1445.

[34]. Nourmohammadi, Z., Joshi, S., Vengallatore, S., Analysis of nonlinear thermoelastic dissipation in Euler–Bernoulli beam resonators, *PLoS ONE,* 11, 10, 2016, e0164669.

[35]. Ma, Q., Clarke, D. R., Size dependent hardness of silver single crystals, *J. Mater. Res.,* 10, 4, 1995, pp. 853–863.

[36]. Gudlavalleti, S., Mechanical Testing of Solid Materials at the Micro-Scale, Ph. D. Thesis, *Massachusetts Institute of Technology*, 2001.

[37]. Cauchy, A., Mémoire sur les systems isotropes de points matériels, Oeuvres complètes. 1re Série – Tome II, *Cambridge University Press*, 1882, pp. 351–386.

[38]. Voigt, W., Theoretische studien über die elasticitätsverhältnisse der krystalle. i. ableitung der grundgleichungen aus der annahme mit polarität begabter moleküle, Abhandlungen der Mathematischen Classe der Königlichen Gesellschaft der Wissenschaften zu Göttingen, *Akademie der Wissenschaften in Göttingen,* 24, 1887, pp. 3–52.

[39]. Nix, W. D., Mechanical properties of thin films, *Metall. Mater. Trans. A*, 20, 11, 1989, pp. 2217–2245.

[40]. Yang, F., Chong, A., Lam, D. C. C., Tong, P., Couple stress based strain gradient theory for elasticity, *Int. J. Solids Struct.,* 39, 10, 2002, pp. 2731–2743.

[41]. Kim, J., Reddy, J., A general third-order theory of functionally graded plates with modified couple stress effect and the von Kármán nonlinearity: theory and finite element analysis, *Acta Mech.*, 226, 9, 2015, pp. 2973–2998.

[42]. Fathalilou, M., Sadeghi, M., Rezazadeh, G., Jalilpour, M., Naghiloo, A. and Ahouighazvin, S., Study on the pull-in instability of gold micro-switches using variable length scale parameter, *Journal of Solid Mechanics,* 3, 2011, pp. 114–123.

[43]. Rahaeifard, M., Kahrobaiyan, M., Asghari, M., Ahmadian, M., Static pull-in analysis of microcantilevers based on the modified couple stress theory, *Sens. Actuat. A,* 171, 2, 2011, pp. 370–374.

[44]. Shaat, M., Mohamed, S., Nonlinear-electrostatic analysis of micro-actuated beams based on couple stress and surface elasticity theories, *Int. J. Mech. Sci.,* 84, 2014, pp. 208–217.

[45]. Asghari, M., Taati, E., A size-dependent model for functionally graded micro-plates for mechanical analyses, *J. Vib. Control*, 19, 11, 2013, pp. 1614–1632.

Published by International Frequency Sensor Association (IFSA) Publishing, S. L., 2019 (http://www.sensorsportal.com).